A DISCONTINUOUS GALERKIN METHOD FOR ELLIPTIC INTERFACE PROBLEMS WITH APPLICATION TO ELECTROPORATION*

GRÉGORY GUYOMARC'H† AND CHANG-OCK LEE‡

Abstract. We present a discontinuous Galerkin (DG) method to solve elliptic interface problems for which discontinuities in the solution and in its normal derivatives are prescribed on an interface inside the domain. Standard ways to solve interface problems with finite element methods consist in enforcing the prescribed discontinuity of the solution in the finite element space. Here, we show that the DG method provides a natural framework to enforce both discontinuities weakly in the DG formulation provided that the triangulation of the domain is fitted to the interface. The resulting discretization leads to a symmetric system that can be efficiently solved with standard algorithms. The method is shown to be optimally convergent in the L^2-norm and numerical experiments are presented to confirm this theoretical result. We apply our method to the numerical study of electroporation, a widely-used medical technique with applications to gene therapy and cancer treatment. Mathematical models of electroporation involves elliptic problems with dynamic interface conditions. We discretize such problems into a sequence of elliptic interface problems that can be solved by our method. We obtain numerical results that agree with known exact solutions.

Key words. discontinuous Galerkin method, elliptic interface problem, electroporation

AMS subject classifications. 65M60, 65N30, 92C37

1. Introduction.

We consider Ω a convex polygonal domain in $\mathbb{R}^2$ and Ω_1 a domain with C^2 boundary such that $\overline{\Omega}_1 \subset \Omega$ (see Figure 1.1). We set $\Gamma_{\rm I} = \partial\Omega_1$ and $\Omega_2 = \Omega \setminus \overline{\Omega}_1$. The domains Ω_1 and Ω_2, and the curve $\Gamma_{\rm I}$ are usually referred as the interior domain, the exterior domain and the interface, respectively. We consider the following elliptic interface problem:

$$-\nabla \cdot \beta \nabla u = f \text{ in } \Omega_1 \cup \Omega_2, \tag{1.1}$$

$$u = g \text{ on } \partial\Omega, \tag{1.2}$$

$$[u] = a\,\mathbf{n} \text{ on } \Gamma_{\rm I}, \tag{1.3}$$

$$[\beta \partial_n u] = b\,\mathbf{n} \text{ on } \Gamma_{\rm I}\,. \tag{1.4}$$

where β is a positive constant on Ω_1 and Ω_2, separately (possibly discontinuous across $\Gamma_{\rm I}$). Here $\mathbf{n}$ is the outward unit normal to $\Gamma_{\rm I}$. The operator ∂_n is the normal derivative defined by $\partial_n u = \nabla u \cdot \mathbf{n}$. We shall emphasize here that $[\cdot]$ takes the standard meaning in discontinuous Galerkin (DG) methods, that is, if we consider K and K' two subdomains of Ω such that $\partial K \cap \partial K' \neq \emptyset$, then for a sufficiently regular scalar function v and vector function $\mathbf{r}$ defined on $K \cup K'$, we define $[v]$ and $[\mathbf{r}]$ on $\partial K \cap \partial K'$ by

$$[v] = v|_K\,\mathbf{n}_K + v|_{K'}\,\mathbf{n}_{K'},$$
$$[\mathbf{r}] = \mathbf{r}|_K \cdot \mathbf{n}_K + \mathbf{r}|_{K'} \cdot \mathbf{n}_{K'},$$

*This work was partially supported by KRF-2002-070-C00004 and KOSEF R01-2000-00008.

†Division of Applied Mathematics, KAIST, Daejeon, 305-701 Korea (gregory@guyomarch.org).

‡Division of Applied Mathematics, KAIST, Daejeon, 305-701 Korea (colee@amath.kaist.ac.kr).

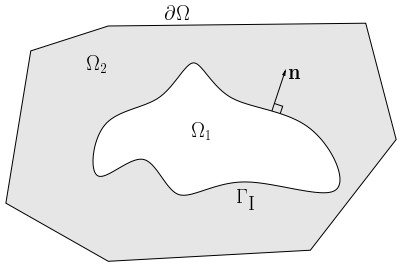

FIG. 1.1: Domain and interface

where $\mathbf{n}_K$ is the outward unit normal to ∂K. On the boundary $\partial\Omega$, we set $[v] = v\mathbf{n}$ and $[\mathbf{r}] = \mathbf{r}\cdot\mathbf{n}$.[1] We also recall the definition of the average operator $\{\cdot\}$:

$$\{v\} = \frac{1}{2}(v|_K + v|_{K'}) \quad \text{on } \partial K \cap \partial K' \qquad \text{and} \qquad \{v\} = v \quad \text{on } \partial\Omega.$$

Several methods exist already to address this problem. The immersed interface method [10] is a finite difference scheme that enforces the jump conditions by an appropriate choice of stencil. The resulting discretization is not symmetric but has second order accuracy. It manages to obtain a sharp solution at the interface contrary to approaches based on singular source terms. Moreover it allows discontinuities in the solution itself, not only in the coefficients. The boundary capturing method [12] is another finite difference scheme with first order accuracy which results in a symmetric system that can be solved with fast Poisson solvers. In fact the resulting linear system is the same as one from a standard discretization of the Poisson equation in the absence of interface (the coefficient β is, however, replaced by an "effective" β to take into account the sub-grid discontinuities). The convergence of the method was shown in [13]. The method was later extended to achieve second order accuracy as described in [8].

There has been also considerable research to solve this problem using finite element methods. In [3], a method is proposed to solve the problem on unfitted meshes (which means the interface is not assumed to exactly lie on the mesh lines), and a complete analysis in the context of variational crimes showed that optimal convergence is achieved thanks to a proper transfer of the boundary conditions from the exact interfaces and boundaries to the approximate ones. The discontinuity in the derivative of u is naturally enforced in the weak formulation while the discontinuity in u is enforced in the finite element space.

In this paper, we present a discontinuous Galerkin method to solve this problem. This is quite a natural approach in the case of a fitted mesh since the approximate solution in a DG discretization is discontinuous across element boundaries. Similarly to the boundary capturing method, the method presented here has the following property: the stiffness matrix resulting from the discretization is the same as one obtained

[1] Usually the jump conditions are given using a different jump operator defined by $[v] = v|_{\Omega_1} - v|_{\Omega_2}$, which is equivalent to ours since one can easily check that on Γ_I

$$[u] = (u|_{\Omega_1} - u|_{\Omega_2})\,\mathbf{n},$$
$$[\beta\partial_n u] = (\beta\,\partial_n(u|_{\Omega_1}) - \beta\,\partial_n(u|_{\Omega_2}))\,\mathbf{n}.$$

by a standard DG discretization of the Poisson problem without jump conditions (the discontinuity terms all appear as extra terms on the right-hand side). Therefore, the resulting linear system can be solved efficiently with standard techniques. It differs from [3] in the sense that both jump conditions are implemented weakly. Moreover, we show that the method can be written in the usual DG form provided we introduce a special choice of fluxes. In this form the convergence of the method can be easily proved using the framework developed in [2].

The standard weak formulation of the problem (1.1)–(1.4) is given below. It can be easily obtained by multiplying (1.1) by a test function v in $H_0^1(\Omega)$, integrating separately on Ω_1 and Ω_2, adding the resulting equations and enforcing the second jump condition (1.4) weakly.

Find u in $H^1(\Omega_1 \cup \Omega_2)$ such that $u = g$ on $\partial\Omega$ and $[u] = a\mathbf{n}$ on Γ_{I} satisfying

$$\int_\Omega \beta\, \nabla u \cdot \nabla v \, dx = \int_\Omega f\, v \, dx + \int_{\Gamma_{\mathrm{I}}} b\, v \, ds \quad \forall v \in H_0^1(\Omega). \tag{1.5}$$

Here, for a bounded open set G in $\mathbb{R}^2$, if $\{D_j\}_{j=1}^m$ are its connected components, we denote by $H^k(G)$ the Sobolev space of functions w such that $w|_{D_j} \in H^k(D_j)$, with the usual broken norm and semi-norm. The source term f is assumed to be in $L^2(\Omega)$, a and g are taken in $H^{3/2}(\Gamma_{\mathrm{I}})$ and $H^{3/2}(\partial\Omega)$, respectively, and b is in $H^{1/2}(\Gamma_{\mathrm{I}})$. We will denote by C a generic constant depending on Ω, Γ_{I} and β. Further dependencies will be denoted by subscripts. We cite without proof the following result obtained in [15] that asserts that problem (1.5) is well-posed:

THEOREM 1.1. *There exists a unique solution of the weak problem (1.5) in $H^2(\Omega_1 \cup \Omega_2)$ which satisfies*

$$\|u\|_{2,\Omega_1\cup\Omega_2} \leq C \left(\|f\|_{0,\Omega} + \|g\|_{\frac{3}{2},\Gamma_{\mathrm{I}}} + \|a\|_{\frac{3}{2},\Gamma_{\mathrm{I}}} + \|b\|_{\frac{1}{2},\Gamma_{\mathrm{I}}} \right). \tag{1.6}$$

2. Discontinuous Galerkin weak formulation. We start by rewriting the problem (1.1)–(1.4) into a first order system as it is usually done in DG methods for elliptic problems. We introduce the auxiliary variable $\mathbf{q}$ in the formulation to obtain the equivalent problem:

$$-\nabla \cdot \left(\sqrt{\beta}\, \mathbf{q} \right) = f \text{ in } \Omega_1 \cup \Omega_2, \tag{2.1}$$

$$\mathbf{q} = \nabla \left(\sqrt{\beta}\, u \right) \text{ in } \Omega_1 \cup \Omega_2, \tag{2.2}$$

$$u = g \text{ on } \partial\Omega, \tag{2.3}$$

$$[u] = a\, \mathbf{n} \text{ across } \Gamma_{\mathrm{I}}, \tag{2.4}$$

$$\left[\sqrt{\beta}\, \mathbf{q} \right] = b \text{ across } \Gamma_{\mathrm{I}}. \tag{2.5}$$

Next, we consider $\mathcal{T}_h = \bigcup K$, a quasi-uniform triangulation of the domain Ω, and we denote by Γ the union of the boundaries of the elements K in $\mathcal{T}_h$. We assume that Γ_{I} is included in Γ (the triangulation is then said to be *fitted* to the interface). We will write Γ_0 for the set of interior edges in Γ that are not interface edges. Therefore, we have the decomposition $\Gamma = \Gamma_0 \cup \Gamma_{\mathrm{I}} \cup \partial\Omega$.

In the first part of this section, we show that the jumps in u and its normal

derivative appear naturally when considering the discontinuous Galerkin formulation of the first order system. This enables us to enforce both jump conditions weakly. In the second part, we show that this amounts to choose fluxes that incorporate the jumps at the interface. The resulting weak problem takes the form of a DG formulation for a standard elliptic problem with a special choice of fluxes. The analysis of the discretization of this weak formulation is the subject of the next section.

2.1. Weakly enforced jump conditions. We start with equation (2.1), multiplying it by a test function v, integrating the result over $K \in \mathcal{T}_h$ and using integration by parts to obtain

$$\int_K \nabla v \cdot \sqrt{\beta}\,\mathbf{q}\,dx - \int_{\partial K} v\sqrt{\beta}\,\mathbf{q}\cdot\mathbf{n}_K\,ds = \int_K f\,v\,dx. \tag{2.6}$$

Summing over all elements K in $\mathcal{T}_h$, we get

$$\sum_{K\in\mathcal{T}_h}\int_K \nabla v \cdot \sqrt{\beta}\,\mathbf{q}\,dx - \sum_{K\in\mathcal{T}_h}\int_{\partial K} v\,\sqrt{\beta}\,\mathbf{q}\cdot\mathbf{n}_K\,ds = \int_\Omega f\,v\,dx. \tag{2.7}$$

We need the following result in [2, eq. (3.3)] in order to transform integrals like the second term in the above equality:

PROPOSITION 2.1. *If φ and $\mathbf{\Psi}$ are functions in $H^1(\mathcal{T}_h)$ and $[H^1(\mathcal{T}_h)]^2$, respectively, then*

$$\sum_{K\in\mathcal{T}_h}\int_{\partial K}\varphi\,\mathbf{\Psi}\cdot\mathbf{n}_K\,ds = \int_\Gamma [\varphi]\cdot\{\mathbf{\Psi}\}\,ds + \int_{\Gamma_0\cup\Gamma_I}\{\varphi\}\,[\mathbf{\Psi}]\,ds.$$

We apply this result to (2.7) setting $\varphi := v$ and $\mathbf{\Psi} := \sqrt{\beta}\,\mathbf{q}$ to obtain

$$\int_\Omega \nabla v\cdot\sqrt{\beta}\,\mathbf{q}\,dx - \int_\Gamma [v]\cdot\left\{\sqrt{\beta}\,\mathbf{q}\right\}ds - \int_{\Gamma_0\cup\Gamma_I}\{v\}\left[\sqrt{\beta}\,\mathbf{q}\right]ds = \int_\Omega f\,v\,dx.$$

Finally, incorporating the jump condition (2.5), we get

$$\int_\Omega \nabla v\cdot\sqrt{\beta}\,\mathbf{q}\,dx - \int_\Gamma [v]\cdot\left\{\sqrt{\beta}\,\mathbf{q}\right\}ds - \int_{\Gamma_0}\{v\}\left[\sqrt{\beta}\,\mathbf{q}\right]ds = \int_\Omega f\,v\,dx + \int_{\Gamma_I} b\,\{v\}\,ds. \tag{2.8}$$

The last step consists in introducing a numerical trace that will approximate the trace of $\sqrt{\beta}\,\mathbf{q}$ on Γ. We use the local discontinuous Galerkin (LDG) trace[2] [6] given below:

$$\widetilde{\sqrt{\beta}\,\mathbf{q}}_e(u,\mathbf{q}) = \left\{\sqrt{\beta}\,\mathbf{q}\right\} - \alpha_e\,([u]) + \begin{cases}\mathbf{0} & \text{if } e\subseteq\Gamma_0\\ \alpha_e\,(a\mathbf{n}) & \text{if } e\subseteq\Gamma_I\\ \alpha_e\,(g\mathbf{n}) & \text{if } e\subseteq\partial\Omega\end{cases}.$$

The penalization term α_e is defined for $\mathbf{\Psi}$ in $\mathbb{R}^2$ by

$$\alpha_e\,(\mathbf{\Psi}) = \frac{\eta}{h_e}\mathbf{\Psi},$$

[2] At this point, one could choose any consistent and conservative DG trace, but we favor the LDG trace because it leads to a symmetric discretization with appropriate stability properties (see [5]).

where η is the penalization parameter and h_e the length of edge e. The penalization term has been modified for interface edges in order to take into account the discontinuity in u. We also assume that the term $\beta_{\mathbf{e}}$ in the LDG method (see [6]) is taken to be $\mathbf{0}$. We omit it for the sake of clarity since the stability of the standard LDG method does not depend upon it. This numerical trace is conservative, which means it is single-valued on Γ, and consequently

$$\widetilde{\left[\sqrt{\beta}\,\mathbf{q}\right]} = 0 \quad \text{and} \quad \widetilde{\left\{\sqrt{\beta}\,\mathbf{q}\right\}} = \widetilde{\sqrt{\beta}\,\mathbf{q}}.$$

Then (2.8) becomes

$$\int_\Omega \nabla v\,\sqrt{\beta}\,\mathbf{q}\,dx - \int_\Gamma [v]\cdot\widetilde{\sqrt{\beta}\,\mathbf{q}}\,ds = \int_\Omega f\,v\,dx + \int_{\Gamma_{\mathrm{I}}} b\,\{v\}\,ds. \tag{2.9}$$

We now proceed in the same way for (2.2), that is, we multiply it by a test function $\mathbf{r}$, integrate over K and use integration by parts to obtain

$$\int_K \mathbf{q}\cdot\mathbf{r}\,dx + \int_K u\,\nabla\cdot\sqrt{\beta}\,\mathbf{r}\,dx - \int_{\partial K} u\,\sqrt{\beta}\,\mathbf{r}\cdot\mathbf{n}_K\,ds = 0. \tag{2.10}$$

Next, summing over all K in $\mathcal{T}_h$ and using Proposition 2.1 with $\varphi := u$ and $\mathbf{\Psi} := \sqrt{\beta}\,\mathbf{r}$, we get

$$\int_\Omega \mathbf{q}\cdot\mathbf{r}\,dx + \int_\Omega u\,\nabla\cdot\sqrt{\beta}\,\mathbf{r}\,dx - \int_\Gamma [u]\cdot\left\{\sqrt{\beta}\,\mathbf{r}\right\}\,ds - \int_{\Gamma_0\cup\Gamma_{\mathrm{I}}} \{u\}\left[\sqrt{\beta}\,\mathbf{r}\right]\,ds = 0.$$

Incorporating the jump condition (2.4), we obtain

$$\begin{aligned}\int_\Omega \mathbf{q}\cdot\mathbf{r}\,dx + \int_\Omega u\,\nabla\cdot\sqrt{\beta}\,\mathbf{r}\,dx - \int_{\Gamma_0\cup\partial\Omega} [u]\cdot\left\{\sqrt{\beta}\,\mathbf{r}\right\}\,ds \\ - \int_{\Gamma_0\cup\Gamma_{\mathrm{I}}} \{u\}\left[\sqrt{\beta}\,\mathbf{r}\right]\,ds = \int_{\Gamma_{\mathrm{I}}} a\,\mathbf{n}\cdot\left\{\sqrt{\beta}\,\mathbf{r}\right\}\,ds.\end{aligned}$$

Finally, we replace u on the edges by the LDG numerical trace:

$$\widetilde{u}_e(u) = \begin{cases}\{u\} & \text{if } e\subseteq\Gamma_0\cup\Gamma_{\mathrm{I}}\\ g & \text{if } e\subseteq\partial\Omega\end{cases}.$$

Here again $\widetilde{u}$ is conservative so that $[\widetilde{u}] = 0$ on $\Gamma_0\cup\Gamma_{\mathrm{I}}$, $[\widetilde{u}] = g\mathbf{n}$ on $\partial\Omega$, and $\{\widetilde{u}\} = \widetilde{u}$ on Γ. Therefore, the last equation can be rewritten as

$$\begin{aligned}\int_\Omega \mathbf{q}\cdot\mathbf{r}\,dx + \int_\Omega u\nabla\cdot\sqrt{\beta}\,\mathbf{r}\,dx - \int_{\Gamma_0\cup\Gamma_{\mathrm{I}}} \widetilde{u}\left[\sqrt{\beta}\,\mathbf{r}\right]\,ds \\ = \int_{\Gamma_{\mathrm{I}}} a\,\mathbf{n}\cdot\left\{\sqrt{\beta}\,\mathbf{r}\right\}\,ds + \int_{\partial\Omega} g\,\mathbf{n}\cdot\left\{\sqrt{\beta}\,\mathbf{r}\right\}\,ds.\end{aligned} \tag{2.11}$$

2.2. Modification of the numerical traces. In this section we answer the question on how to modify $\widetilde{u}$ and $\widetilde{\sqrt{\beta}\,\mathbf{q}}$ so that when we replace u and $\sqrt{\beta}\,\mathbf{q}$ in the edge integrals in (2.6) and (2.10) by their modified numerical traces, we obtain

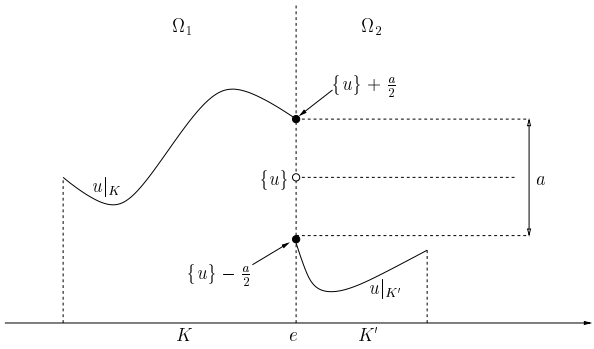

FIG. 2.1: Consistency of $\hat{u}$

two equations that lead to (2.9) and (2.11), respectively. It is easy to check using Remark 2.3 that a possible choice of traces is given by

$$\widehat{u}_{K,e}(u) = \widetilde{u}_e(u) + \begin{cases} 0 & \text{if } e \subseteq \Gamma_0 \cup \partial\Omega \\ \frac{1}{2}\,a & \text{if } e \subseteq \Gamma_{\rm I} \text{ and } K \subseteq \Omega_1 \\ -\frac{1}{2}\,a & \text{if } e \subseteq \Gamma_{\rm I} \text{ and } K \subseteq \Omega_2 \end{cases}$$

and

$$\widehat{\sqrt{\beta}\,\mathbf{q}}_{K,e}(u,\mathbf{q}) = \widetilde{\sqrt{\beta}\,\mathbf{q}}_e(u,\mathbf{q}) + \begin{cases} 0 & \text{if } e \subseteq \Gamma_0 \cup \partial\Omega \\ \frac{1}{2}\,b\,\mathbf{n} & \text{if } e \subseteq \Gamma_{\rm I} \text{ and } K \subseteq \Omega_1 \\ -\frac{1}{2}\,b\,\mathbf{n} & \text{if } e \subseteq \Gamma_{\rm I} \text{ and } K \subseteq \Omega_2 \end{cases}.$$

Note that these traces are identical to the LDG traces whenever the edge e is not a part of the interface. If e is a part of the interface, then a term independent of u and $\mathbf{q}$ is added to take into account the prescribed discontinuities. This choice of fluxes satisfies a certain form of consistency that is contained in the following remarks.

REMARK 2.2. *If u is the solution of the problem as given by Theorem 1.1 then*

$$\widehat{u}_{K,e}(u) = u, \qquad \widehat{\sqrt{\beta}\,\mathbf{q}}_{K,e}\left(u, \sqrt{\beta}\,\nabla u\right) = \beta\,\nabla u \qquad \textit{when } e \subseteq \Gamma_0 \cup \partial\Omega,$$

$$\widehat{u}_{K,e}(u) = u|_{\Omega_i|_e}, \quad \widehat{\sqrt{\beta}\,\mathbf{q}}_{K,e}\left(u, \sqrt{\beta}\,\nabla u\right) \cdot \mathbf{n} = (\beta\,\nabla u \cdot \mathbf{n})\,|_{\Omega_i|_e} \qquad \textit{when } e \subseteq \Gamma_{\rm I}\,.$$

These relations can be checked by straightforward computations, and Figure 2.1 gives a graphical interpretation.

REMARK 2.3. *It follows directly from the definition of $\widehat{u}$ and $\widehat{\sqrt{\beta}\,\mathbf{q}}$ that*

$$[\widehat{u}] = \begin{cases} \mathbf{0} & \textit{on } \Gamma_0 \\ g\,\mathbf{n} & \textit{on } \partial\Omega \\ a\,\mathbf{n} & \textit{on } \Gamma_{\rm I} \end{cases} \qquad \textit{and} \qquad \left[\widehat{\sqrt{\beta}\,\mathbf{q}}\right] = \begin{cases} 0 & \textit{on } \Gamma_0 \\ \sqrt{\beta}\,\mathbf{q}\cdot\mathbf{n} & \textit{on } \partial\Omega \\ b & \textit{on } \Gamma_{\rm I} \end{cases}.$$

In addition, $\{\widehat{u}\} = \{u\}$ *on* $\Gamma_0 \cup \Gamma_{\rm I}$ *and*

$$\left\{\widehat{\sqrt{\beta}\,\mathbf{q}}\right\} = \left\{\sqrt{\beta}\,\mathbf{q}\right\} - \alpha_e\,([u]) + \begin{cases} \mathbf{0} & on\ \Gamma_0 \\ \alpha_e\,(g\,\mathbf{n}) & on\ \partial\Omega\ . \\ \alpha_e\,(a\,\mathbf{n}) & on\ \Gamma_{\rm I} \end{cases}$$

With this definition of numerical traces, the weak formulation takes the standard form:

Find u *in* $H^1(\mathcal{T}_h)$ *and* $\mathbf{q}$ *in* $\left[H^1(\mathcal{T}_h)\right]^2$ *such that for all* K *in* $\mathcal{T}_h$

$$\begin{aligned} \int_K \mathbf{q}\cdot\mathbf{r}\,dx + \int_K u\,\nabla\cdot\sqrt{\beta}\,\mathbf{r}\,dx - \int_{\partial K}\widehat{u}\,\sqrt{\beta}\,\mathbf{r}\cdot\mathbf{n}_K\,ds = 0 \qquad & \forall \mathbf{r}\in\left[H^1(K)\right]^2, \\ \int_K \nabla v\cdot\sqrt{\beta}\,\mathbf{q}\,dx - \int_{\partial K} v\,\widehat{\sqrt{\beta}\,\mathbf{q}}\cdot\mathbf{n}_K\,ds = \int_K f\,v\,dx \quad & \forall v\in H^1(K). \end{aligned}$$

3. Primal form and error estimates. In this section, we analyze the DG discretization of the weak problem obtained in the previous section. As usual in DG methods, we approximate $H^1(\mathcal{T}_h)$ and $[H^1(\mathcal{T}_h)]^2$ by the spaces $\mathcal{V}_h$ and $\mathcal{M}_h$ defined by

$$\begin{aligned} \mathcal{V}_h &= \{v\in L^2(\Omega)\,:\, v|_K\in\mathcal{P}(K) \text{ for all } K \text{ in } \mathcal{T}_h\}, \\ \mathcal{M}_h &= \{\mathbf{r}\in\left[L^2(\Omega)\right]^2\,:\, \mathbf{r}|_K\in[\mathcal{P}(K)]^2 \text{ for all } K \text{ in } \mathcal{T}_h\}, \end{aligned}$$

where $\mathcal{P}(K) = \mathcal{P}_l(K)$ is the space of polynomial functions of degree at most $l \geq 1$ on K. The discrete problem is then given by:

Find u_h *in* $\mathcal{V}_h$ *and* $\mathbf{q}_h$ *in* $\mathcal{M}_h$ *such that for all* K *in* $\mathcal{T}_h$

$$\int_K \mathbf{q}_h\cdot\mathbf{r}\,dx + \int_K u_h\,\nabla\cdot\sqrt{\beta}\,\mathbf{r}\,dx - \int_{\partial K}\widehat{u}\,\sqrt{\beta}\,\mathbf{r}\cdot\mathbf{n}_K\,ds = 0 \quad \forall \mathbf{r}\in[\mathcal{P}(K)]^2, \tag{3.1}$$

$$\int_K \nabla v\cdot\sqrt{\beta}\,\mathbf{q}_h\,dx - \int_{\partial K} v\,\widehat{\sqrt{\beta}\,\mathbf{q}}\cdot\mathbf{n}_K\,ds = \int_K f\,v\,dx \qquad \forall v\in\mathcal{P}(K). \tag{3.2}$$

We first derive the primal form associated with this discretization. Since it takes basically the same form as a DG discretization for a standard elliptic problem, the primal form is easily obtained within the framework developed in [2]. Moreover, only slight modifications of the proof in [2] of boundedness and stability of the LDG method are required to show our main result stated below.

THEOREM 3.1. *If* $u_h\in\mathcal{V}_h$ *is the piecewise linear solution of (3.1) and (3.2) and* $u\in H^2(\Omega_1\cup\Omega_2)$ *is the exact solution as given by Theorem 1.1, then*

$$\|u-u_h\|_{0,\Omega_1\cup\Omega_2} \leq C\,h^2\left(\|f\|_{0,\Omega} + \|g\|_{\frac{3}{2},\Gamma_{\rm I}} + \|a\|_{\frac{3}{2},\Gamma_{\rm I}} + \|b\|_{\frac{1}{2},\Gamma_{\rm I}}\right).$$

The proof of this theorem will be given in the last part of this section.

3.1. Primal form. We proceed as in Section 2.1 using Proposition 2.1 for equations (3.1) and (3.2) to obtain

$$\int_\Omega \mathbf{q}_h \cdot \mathbf{r}\, dx + \int_\Omega u_h\, \nabla\cdot \sqrt{\beta}\,\mathbf{r}\, dx - \int_\Gamma [\widehat{u}]\cdot\left\{\sqrt{\beta}\,\mathbf{r}\right\} ds - \int_{\Gamma_0\cup\Gamma_I} \{\widehat{u}\}\left[\sqrt{\beta}\,\mathbf{r}\right] ds = 0, \tag{3.3}$$

$$\int_\Omega \nabla v\cdot\sqrt{\beta}\,\mathbf{q}_h\, dx - \int_\Gamma [v]\cdot\left\{\widehat{\sqrt{\beta}\,\mathbf{q}}\right\} ds - \int_{\Gamma_0\cup\Gamma_I} \{v\}\left[\widehat{\sqrt{\beta}\,\mathbf{q}}\right] ds = \int_\Omega f\, v\, dx. \tag{3.4}$$

We recall the following integration by parts formula from [2, eq. (3.6)]:

PROPOSITION 3.2. *If φ and $\mathbf{\Psi}$ are functions in $H^1(\mathcal{T}_h)$ and $[H^1(\mathcal{T}_h)]^2$, respectively, then*

$$-\int_\Omega \varphi\,\nabla\cdot\mathbf{\Psi}\, dx = \int_\Omega \nabla\varphi\cdot\mathbf{\Psi}\, dx - \int_\Gamma [\varphi]\cdot\{\mathbf{\Psi}\}\, ds - \int_{\Gamma_0\cup\Gamma_I}\{\varphi\}\,[\mathbf{\Psi}]\, ds.$$

We apply this proposition with $\varphi := u_h$ and $\mathbf{\Psi} := \sqrt{\beta}\,\mathbf{r}$ to (3.3) to obtain

$$\int_\Omega \mathbf{q}_h\cdot\mathbf{r}\, dx = \int_\Omega \nabla u_h\cdot\sqrt{\beta}\,\mathbf{r}\, dx + \int_\Gamma [\widehat{u}-u_h]\cdot\left\{\sqrt{\beta}\,\mathbf{r}\right\} ds. \tag{3.5}$$

where we have used the fact that $\{\widehat{u}(u_h)-u_h\}=0$ on $\Gamma_0\cup\Gamma_I$ by definition of $\widehat{u}$. We need the following lifting operator l to get rid of the edge integral in (3.5).

DEFINITION 3.3. *For τ in $\left[L^2(\Gamma)\right]^2$, we define $l(\tau)$ to be the function in $\mathcal{M}_h$ such that*

$$\int_\Omega l(\tau)\cdot\mathbf{\Psi}\, dx = -\int_\Gamma \tau\cdot\{\mathbf{\Psi}\}\, ds \quad \textit{for all } \mathbf{\Psi} \textit{ in } \mathcal{M}_h.$$

Setting $\tau := [\widehat{u}-u_h]$ and $\mathbf{\Psi} := \sqrt{\beta}\,\mathbf{r}$, we can rewrite (3.5) as

$$\int_\Omega \mathbf{q}_h\cdot\mathbf{r}\, dx = \int_\Omega \nabla u_h\cdot\sqrt{\beta}\,\mathbf{r}\, dx - \int_\Omega l\left([\widehat{u}-u_h]\right)\cdot\sqrt{\beta}\,\mathbf{r}\, dx.$$

For this equation to be true for all $\mathbf{r}$ in $\mathcal{M}_h$, we must have

$$\mathbf{q}_h = \sqrt{\beta}\left(\nabla u_h - l\left([\widehat{u}-u_h]\right)\right). \tag{3.6}$$

Finally, substituting (3.5) into (3.4) with $\mathbf{r} := \sqrt{\beta}\,\nabla v$, we obtain

$$\int_\Omega \beta\,\nabla u_h\cdot\nabla v\, dx + \int_\Gamma [\widehat{u}-u_h]\cdot\{\beta\,\nabla v\}\, ds - \int_\Gamma [v]\cdot\left\{\widehat{\sqrt{\beta}\,\mathbf{q}}\right\} ds - \int_{\Gamma_0\cup\Gamma_I}\{v\}\left[\widehat{\sqrt{\beta}\,\mathbf{q}}\right] ds = \int_\Omega f\, v\, dx. \tag{3.7}$$

Now using Remark 2.3 along with (3.6) and the Definition 3.3 of the lifting operator l, (3.7) can be further simplified to lead to the primal formulation of our problem:

Find u_h in $\mathcal{V}_h$ such that

$$\mathcal{A}(u_h, v) = \mathcal{L}(v) \quad \forall v\in\mathcal{V}_h$$

where

$$\mathcal{A}(u,v) = \int_\Omega \beta\,\nabla u\cdot\nabla v\,dx - \int_\Gamma \left([u]\cdot\{\beta\,\nabla v\} + [v]\cdot\{\beta\,\nabla u\}\right) ds + \int_\Omega \beta\, l\left([u]\right)\cdot l\left([v]\right)\,dx + \alpha\left([u],[v]\right) \quad (3.8)$$

and

$$\mathcal{L}(v) = \int_\Omega f\,v\,dx + \int_{\Gamma_{\rm I}} b\,\{v\}\,ds - \int_{\Gamma_{\rm I}} a\mathbf{n}\cdot\{\beta\,\nabla v\}\,ds - \int_{\partial\Omega} g\mathbf{n}\cdot\{\beta\,\nabla v\}\,ds + \int_\Omega \beta\, l\left(\bar a\mathbf{n}+\bar g\mathbf{n}\right)\cdot l\left([v]\right)dx - \alpha\left(\bar a\mathbf{n}+\bar g\mathbf{n},[v]\right) \quad (3.9)$$

with the jump operator α defined by

$$\alpha(\mathbf{\Psi}_1,\mathbf{\Psi}_2) = \sum_{e\in\Gamma}\int_e \frac{\eta}{h_e}\mathbf{\Psi}_1\cdot\mathbf{\Psi}_2.$$

In (3.9), $\bar a$ and $\bar g$ are extensions of a and g, respectively, to the whole Γ obtained by setting $\bar a := 0$ on $\Gamma\setminus\Gamma_{\rm I}$ and $\bar g := 0$ on $\Gamma\setminus\partial\Omega$, so that we can use the lifting operator l and the jump operator α.

3.2. Boundedness and stability. Because the bilinear form $\mathcal{A}$ is the same as the bilinear form of the LDG method in [2] with $\beta := 1$, most of the analysis carried in [2] works for $\mathcal{A}$ as well. However, special care should be taken in order to have the boundedness of $\mathcal{A}$ in a space that includes the exact solution u given by Theorem 1.1 if we wish to obtain a priori error estimates. We consider the space X given by

$$X = \mathcal{V}_h + H^2(\Omega_1\cup\Omega_2)$$

with the norm

$$\|v\|_X^2 = |v|_{1,\mathcal{T}_h}^2 + \sum_{K\in\mathcal{T}_h} h_K^2\,|v|_{2,K}^2 + |v|_*^2$$

where

$$|v|_*^2 = \sum_{e\in\Gamma} h_e^{-1}\|\,[v]\,\|_{0,e}^2.$$

Noticing that $|v|_* = 0$ implies $v|_{\partial\Omega}= 0$ and $[v] = 0$ on $\Gamma_0\cup\Gamma_{\rm I}$, from which one can easily prove that $v\in H^1(\Omega)$, we conclude that $\|\cdot\|_X$ is indeed a norm on X. We will also need the following norm on $\mathcal{V}_h$:

$$\|v\|_h^2 = |v|_{1,\mathcal{T}_h}^2 + |v|_*^2\,.$$

We will obtain stability on $\mathcal{V}_h$ in $\|\cdot\|_h$ and boundedness on X in $\|\cdot\|_X$ (note that these norms are equivalent on the approximation space $\mathcal{V}_h$ as can be seen from a standard inverse inequality). We start to show that $\mathcal{A}$ is a bounded bilinear functional for this last norm, proceeding term by term. It is clear that for u, v in X

$$\left|\int_\Omega \beta\,\nabla u\cdot\nabla v\,dx\right| \le C\,|u|_{1,\mathcal{T}_h}\,|v|_{1,\mathcal{T}_h} \quad (3.10)$$

and

$$|\alpha([u],[v])| \leq \eta\ |u|_*\,|v|_*\,. \tag{3.11}$$

We need the following lemma in order to bound the third term in (3.8):

LEMMA 3.4. *If* $\mathbf{\Psi}$ *is in* $\left[L^2(\Gamma)\right]^2$ *then*

$$\|l(\mathbf{\Psi})\|_{0,\Omega}^2 \leq C\sum_{e\in\Gamma} h_e^{-1}\|\mathbf{\Psi}\|_{0,e}^2.$$

Proof. Using the arguments in [2, p. 1763], we obtain the results. □

Applying this lemma to $\mathbf{\Psi} := [v]$ gives

$$\|l([v])\|_{0,\Omega} \leq C\ |v|_*\,, \tag{3.12}$$

which implies

$$\left|\int_\Omega l([u])\cdot l([v])\ dx\right| \leq C\ |u|_*\ |v|_*\,. \tag{3.13}$$

For the remaining term, we need the following inequality in [1, eq. (2.5)] for a function φ in $H^2(K)$:

$$\|\partial_n\varphi\|_{0,e}^2 \leq C\left(h_e^{-1}\,|\varphi|_{1,K}^2 + h_e\,|\varphi|_{2,K}^2\right), \tag{3.14}$$

where C depends on the minimum angle bound of the mesh. First, observe that

$$|\{\nabla v\}\cdot[u]| = |\{\partial_n v\}|\,|[u]|$$

because $[u]$ is collinear to $\mathbf{n}$, and therefore

$$\left|\int_\Gamma \{\beta\,\nabla v\}\cdot[u]\ ds\right| \leq C\sum_{e\in\Gamma}\int_e |\{\partial_n v\}|\,|[u]|\ ds$$

where β has been incorporated in the constant C. Next, apply Cauchy-Schwarz inequality to get

$$\begin{aligned}\left|\int_\Gamma \{\beta\,\nabla v\}\cdot[u]\ ds\right| &\leq C\sum_{e\in\Gamma}\|\,\{\partial_n v\}\,\|_{0,e}\|\,[u]\,\|_{0,e}\\ &\leq C\sum_{e\in\Gamma}\left(\|\partial_n(v|_K)\|_{0,e} + \|\partial_n(v|_{K'})\|_{0,e}\right)\|\,[u]\,\|_{0,e}\end{aligned}$$

where K and K' are the two adjacent triangles with common edge e. The last inequality results from the definition of $\{\cdot\}$. Using (3.14), it follows that

$$\left|\int_\Gamma \{\beta\,\nabla v\}\cdot[u]\ ds\right| \leq C\sum_{e\in\Gamma}\left(\|\,[u]\,\|_{0,e}\sum_{K\in\mathcal{T}_h, e\subset\partial K}\left(h_e^{-1}\,|v|_{1,K}^2 + h_e\,|v|_{2,K}^2\right)^{\frac{1}{2}}\right).$$

Factorizing h_e^{-1}, noting that $h_e \leq h_K$ (h_K being the maximum of all h_e when e belongs to ∂K) and using the Cauchy-Schwarz inequality again, we finally obtain

$$\begin{aligned}\left|\int_\Gamma \{\beta\,\nabla v\}\cdot[u]\ ds\right|^2 &\leq C\left(\sum_{e\in\Gamma} h_e^{-1}\|\,[u]\,\|_{0,e}^2\right)\left(\sum_{K\in\mathcal{T}_h}|v|_{1,K}^2 + h_K^2\,|v|_{2,K}^2\right)\\ &\leq C\,|u|_*^2\ \|v\|_X^2.\end{aligned} \tag{3.15}$$

Combining (3.10), (3.11), (3.13) and (3.15), we have the boundedness of $\mathcal{A}$ in X:

$$\forall u, v \in X \quad |\mathcal{A}(u,v)| \leq C\|u\|_X \|v\|_X.$$

We now recall from [2] how to obtain the coercivity of $\mathcal{A}$ in $\mathcal{V}_h$ for arbitrary $\eta > 0$. First, we remark that for any v in $\mathcal{V}_h$, we have

$$\mathcal{A}(v,v) = \int_\Omega \beta \left|\nabla v + l([v])\right|^2 dx + \alpha([v],[v]).$$

Hence,

$$\mathcal{A}(v,v) \geq C\left(|v|^2_{1,\mathcal{T}_h} + \int_\Omega \nabla v \cdot l([v])\, dx + \|l([v])\|^2_{0,\Omega}\right) + \eta\,|v|^2_*.$$

For any $0 < \epsilon < 1$, apply the arithmetic-geometric mean inequality to the second term in the parenthesis to obtain

$$\mathcal{A}(v,v) \geq C\left(|v|^2_{1,\mathcal{T}_h}(1-\epsilon) + \|l([v])\|^2_{0,\Omega}\left(1 - \frac{1}{\epsilon}\right)\right) + \eta\,|v|^2_*,$$

and using (3.12) we have

$$\mathcal{A}(v,v) \geq C\,|v|^2_{1,\mathcal{T}_h}(1-\epsilon) + \left(C\left(1-\frac{1}{\epsilon}\right) + \eta\right)|v|^2_*.$$

Since the above inequality is valid when ϵ is taken arbitrarily close to 1, we conclude the stability of $\mathcal{A}$ in $\mathcal{V}_h$ for any $\eta > 0$:

$$\mathcal{A}(v,v) \geq C_\eta \|v\|^2_h.$$

3.3. Error estimates. We first start by noting that if u in $H^2(\Omega_1 \cup \Omega_2)$ is the exact solution of the problem as given by Theorem 1.1, then we have the consistency result:

$$\mathcal{A}(u,v) = \mathcal{L}(v) \quad \forall v \in \mathcal{V}_h.$$

This can be easily obtained using Remark 2.2. Hence the Galerkin orthogonality property holds:

$$\mathcal{A}(u - u_h, v) = 0 \quad \forall v \in \mathcal{V}_h.$$

We quote the following approximation property from [2, eq. (4.22)]:

PROPOSITION 3.5. *For $p \geq 0$, if u is a function in $H^{p+1}(\mathcal{T}_h)$ and u_I is its piecewise polynomial interpolant of degree at most p, then*

$$\|u - u_I\|_X \leq Ch^p\,|u|_{p+1,\mathcal{T}_h}$$

where C depends on the minimum angle of the elements in the partition $\mathcal{T}_h$.

If we assume that the solution u is in $H^{p+1}(\mathcal{T}_h)$ for some $p \geq 1$ then

$$\begin{aligned} C_1\|u_I - u_h\|^2_X \leq \mathcal{A}(u_I - u_h, u_I - u_h) &= \mathcal{A}(u_I - u, u_I - u_h) \\ &\leq C_2\|u_I - u\|_X \|u_I - u_h\|_X. \end{aligned}$$

Hence,

$$\begin{aligned}\|u-u_h\|_X &\le \|u-u_I\|_X + \|u_I-u_h\|_X \\ &\le C\|u-u_I\|_X,\end{aligned}$$

and finally by Proposition 3.5, we have

$$\|u-u_h\|_X \le Ch^p\,|u|_{p+1,\mathcal{T}_h}\,. \tag{3.16}$$

Using the standard duality argument, we obtain L^2-error estimates. If φ is the solution of

$$\begin{cases} -\nabla\cdot\beta\,\nabla\varphi = u-u_h & \text{in } \Omega \\ \varphi = 0 & \text{on } \partial\Omega \end{cases}$$

then it must satisfy

$$\mathcal{A}\,(\varphi, v) = \int_\Omega (u-u_h)\,v\,dx \quad \forall v\in X$$

because $\mathcal{A}$ is in fact the bilinear form for the standard elliptic problem (without jump conditions). We denote by φ_I the piecewise linear interpolant of φ, setting $v := u-u_h$ in the above inequality, we have

$$\begin{aligned}\|u-u_h\|^2_{0,\Omega} &= \mathcal{A}(\varphi, u-u_h) \\ &= \mathcal{A}(\varphi-\varphi_I, u-u_h) \\ &\le C\|\varphi-\varphi_I\|_X\|u-u_h\|_X && \text{(boundedness of } \mathcal{A} \text{ in } X) \\ &\le Ch\,|\varphi|_{2,\Omega}\,\|u-u_h\|_X && \text{(Proposition 3.5)} \\ &\le Ch\|u-u_h\|_{0,\Omega}\|u-u_h\|_X && \text{(elliptic regularity)} \\ &\le Ch^2\|u-u_h\|_{0,\Omega}\,|u|_{2,\mathcal{T}_h} && \text{(see (3.16))} \\ &\le Ch^2\|u-u_h\|_{0,\Omega}\,|u|_{2,\Omega_1\cup\Omega_2}\,. && \text{(u is in } H^2(\Omega_1\cup\Omega_2)\text{)}\end{aligned}$$

Theorem 3.1 is then a direct consequence of this last inequality and the regularity estimate (1.6).

4. Numerical experiments. We performed a number of numerical experiments to check the theoretical order of convergence. We present some of the examples presented in [12] and [8]. The triangular meshes used in these simulations were generated using the constraint Delaunay triangulation capabilities of the software *Triangle* which can be obtained freely on its web site [16].

4.1. Standard example. This example can be found in [12] and was actually proposed in [11]. It shows the case of a rather complex interface. Here and in the following examples, we give only the domain, the description of the interface as a parametric curve, the coefficient β in both Ω_1 and Ω_2, and the exact solution u. It is then easy to derive the corresponding jump conditions a and b, the Dirichlet condition

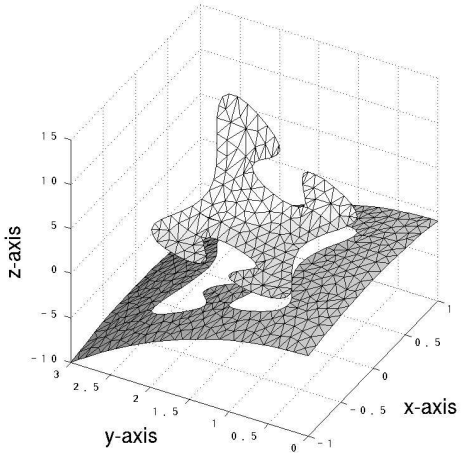

FIG. 4.1: Numerical solution for Example 4.1

TABLE 4.1: Convergence of the method for Example 4.1

Element	Degrees of freedom	Relative L^2-error in u		Relative H^1-error in u	
		Error	Reduction order	Error	Reduction order
$\mathcal{P}_1$	222	9.1889e-03	-	1.1085e-01	-
	792	1.5478e-03	2.569	4.4439e-02	1.318
	3066	4.2667e-04	1.859	2.2576e-02	0.977
	12246	1.1081e-04	1.945	1.1329e-02	0.994
	48840	2.6515e-05	2.063	5.4103e-03	1.066
$\mathcal{P}_2$	444	2.3174e-04	-	5.5694e-03	-
	1584	3.1645e-05	2.872	1.6743e-03	1.733
	6132	6.5529e-06	2.271	6.2315e-04	1.425
	24492	7.6568e-07	3.097	1.5223e-04	2.033
	97680	8.3150e-08	3.202	3.5610e-05	2.095

g and the source term f.

$$\Omega = [-1,1] \times [0,3]$$

$$\Gamma_{\mathrm{I}}(\theta) = \begin{pmatrix} 0.6\cos\theta - 0.3\cos 3\theta \\ 1.5 + 0.7\sin\theta - 0.07\sin 3\theta + 0.2\sin 7\theta \end{pmatrix} \text{ for } \theta \text{ in } [0, 2\pi]$$

$$u(x,y) = \begin{cases} e^x(y^2 + x^2\sin y) & \text{in } \Omega_1 \\ -(x^2+y^2) & \text{in } \Omega_2 \end{cases}$$

$$\beta = \begin{cases} 1 & \text{in } \Omega_1 \\ 10 & \text{in } \Omega_2 \end{cases}$$

We also give in Figure 4.1 a plot of the numerical solution. The convergence results are gathered in Table 4.1. We used a sequence of mesh where each time the number of elements was multiplied by 4 approximately. This roughly amounts to divide the

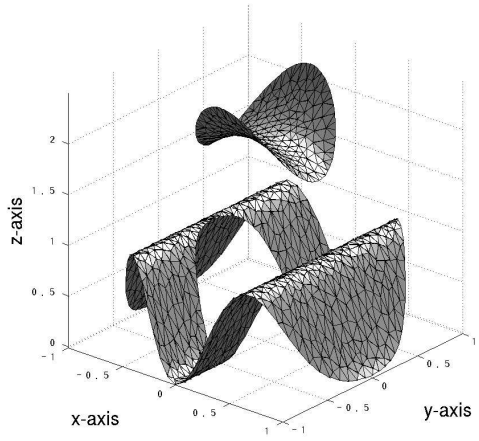

FIG. 4.2: Numerical solution for Example 4.2

TABLE 4.2: Convergence of the method for Example 4.2

Element	Degrees of freedom	Relative L^2-error in u		Relative H^1-error in u	
		Error	Reduction order	Error	Reduction order
$\mathcal{P}_1$	318	2.0171e-02	-	3.4851e-01	-
	1332	4.5803e-03	2.138	1.4959e-01	1.220
	5250	1.1583e-03	1.983	7.5754e-02	0.981
	21276	2.5614e-04	2.177	3.6423e-02	1.056
	84390	6.4070e-05	1.999	1.8144e-02	1.005
$\mathcal{P}_2$	636	2.9975e-03	-	8.6147e-02	-
	2664	2.5744e-04	3.541	1.8791e-02	2.196
	10500	3.2786e-05	2.973	4.8007e-03	1.968
	42552	4.0515e-06	3.016	1.1864e-03	2.016
	168780	4.9652e-07	3.028	2.9531e-04	2.006

mesh size h by 2. We note that the results are as expected, we get order 2 in the L^2-norm with piecewise linear approximation and order 3 with piecewise quadratic approximation, and one order less in the H^1-norm.

4.2. Strong discontinuity in the coefficient β. This example is adapted from [8]. We consider a strong discontinuity in the coefficient β across the interface Γ_{I}. This leads to a poorly conditioned linear system that requires significantly more preconditioned conjugate gradient iterations to converge. However, as can be seen from Table 4.2, the orders of convergence are the same and agree with the theoretical analysis.

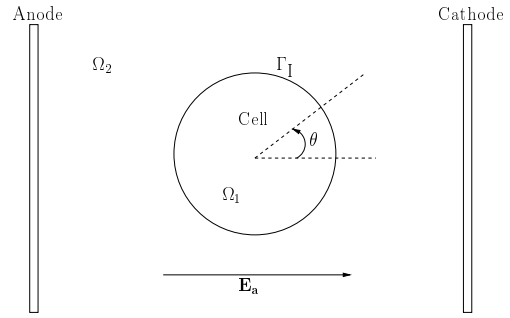

FIG. 5.1: Model of a cell in an electric field

$$\begin{aligned}
\Omega &= \text{ Circle of radius 1 with center at origin} \\
\Gamma_I &= \text{ Circle of radius } \frac{1}{2} \text{ with center at origin} \\
u(x,y) &= \begin{cases} 2y^2 - 2x^2 + 2 & \text{in } \Omega_1 \\ (\sin 3x)^2 & \text{in } \Omega_2 \end{cases} \\
\beta &= \begin{cases} 1000 & \text{in } \Omega_1 \\ 1 & \text{in } \Omega_2 \end{cases}
\end{aligned}$$

5. Computation of the transmembrane voltage of a biological cell. We use our method for the computation of the induced voltage in a cell when a strong electric pulse is applied. This has important applications in the study of electroporation, a widely-use technique for the introduction of chemical species in biological cells. After briefly describing the electroporation phenomenon, we present the mathematical model used in our simulation and suggest a discretization that reduces this model to a sequence of elliptic interface problems that can be solved by our method. Finally, we present numerical results for the potential induced by a spherical cell when exposed to a rectangular pulse.

5.1. Electroporation. The goal of electroporation is to make the cell membrane temporarily permeable to allow chemical species (drugs or engineered genes) in the extracellular medium to pass through and enter the cytoplasm. This is achieved by exposing the cell to a strong electric pulse (rectangular or exponentially decaying). This process is illustrated in Figure 5.1. The fundamental biophysics of electroporation is not yet completely understood, and mathematical models are still under development. Recent models are difficult to solve analytically and therefore require numerical experiments for their validation. A concise review of electroporation and a rather comprehensive source of references can be found in [7].

5.2. A mathematical model. Our main interest is the study of the time evolution of the sub-threshold transmembrane potential (the discontinuity of the electric potential across the membrane). That is, we assume that electroporation has not yet started and we may only consider the physical behavior of the cell. Indeed, when we expose a cell to an electric pulse $\mathbf{E_a}$, the induced electric field $\mathbf{E_i}$ is such that the potential V_i, from which this electric field is derived, is discontinuous across the membrane. When this discontinuity reaches a certain threshold, the electrical behavior of the cell membrane is no longer one of a conductor because of the formation

TABLE 5.1: Electrical and geometrical parameters

Symbol	Value	Definition
r	$10^{-6}\ m$	Cell radius
R_m	$1.66\ 10^{-2}\ \Omega \cdot m^2$	Membrane resistivity
C_m	$0.88\ 10^{-2}\ F/m^2$	Membrane capacitance
σ_1	$3.00\ 10^{-1}\ S/m$	Cytoplasmic conductivity
σ_2	$3.00\ 10^{-1}\ S/m$	Extracellular medium conductivity
E_a	$10^5\ V/m$	Amplitude of electric pulse

of nano-scale pores in the membrane. However, until this critical time, the Maxwell theory of electromagnetism can be applied to determine $\mathbf{E_i}$.

Due to a significant difference of magnitude between the membrane thickness d (typically of the order of 5nm) and the cell radius r (around 10μm for a spherical cell), it is advantageous to consider a macroscale model of the membrane. In the limit case of a very thin membrane ($d \ll r$), the macroscale model [4] is given by

$$-\nabla \cdot \sigma \nabla V = 0 \text{ in } \Omega_1 \cup \Omega_2, \tag{5.1}$$

$$V = V_a \text{ on } \partial\Omega, \tag{5.2}$$

$$[\sigma \partial_n V] = \mathbf{0} \text{ on } \Gamma_{\mathrm{I}}, \tag{5.3}$$

$$C_m \frac{\partial [V]}{\partial t} + \frac{1}{R_m} [V] = -\sigma_1 \, \partial_n \left(V|_{\Omega_1} \right) \mathbf{n} \text{ on } \Gamma_{\mathrm{I}}, \tag{5.4}$$

$$[V]_{(t=0)} = \mathbf{0} \text{ on } \Gamma_{\mathrm{I}}, \tag{5.5}$$

where V is the electric potential (the sum of the applied potential V_a and the induced potential V_i), σ is the conductivity and is divided into σ_1, the cytoplasmic conductivity, and σ_2, the extracellular medium conductivity, C_m is the membrane capacitance, and R_m is the membrane resistivity. Here we consider that $\partial\Omega$ is sufficiently far from the cell where we may assume that the applied electrical field $\mathbf{E_a}$ is not perturbed and we can take the Dirichlet boundary condition $V = V_a$ on $\partial\Omega$ where V_a is such that $-\nabla V_a = \mathbf{E_a}$. The values for electrical and geometrical parameters are given in Table 5.1 and are adapted from [9]. Note that (5.1) is the conservation of current

$$\nabla \cdot \mathbf{j} = \frac{\partial \rho}{\partial t} \tag{5.6}$$

in the absence of sources (the right-hand side of (5.6) is taken to be zero), where $\mathbf{j} = \sigma \mathbf{E}$ is the electric current and ρ the charge density. The current $\mathbf{j}$ is continuous across the membrane as expressed by (5.3) but the potential is discontinuous and the discontinuity is driven by the evolution equation (5.4). This equation is strongly coupled with the Laplace equation (5.1) through its right-hand side and cannot be solved independently.

5.3. Discretization. The problem (5.1)–(5.4) can be viewed as a sequence of elliptic problems with interface, provided we discretize (5.4) with a forward Euler time-step:

$$C_m \frac{\left[V^{p+1}\right] - [V^p]}{\Delta t} + \frac{1}{R_m} [V^p] = -\sigma_1 \, \partial_n \left(V^p|_{\Omega_1} \right) \mathbf{n}. \tag{5.7}$$

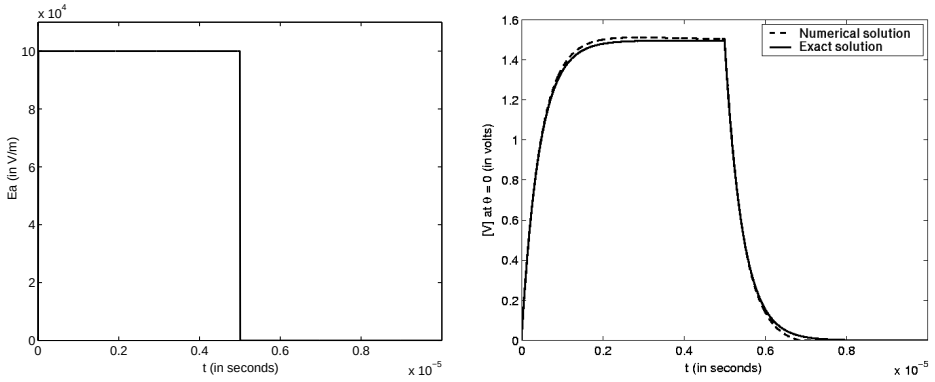

Applied electric pulse E_a Transmembrane voltage $[V]$

FIG. 5.2: Cell response to a rectangular electric pulse

We start by solving (5.1) with our method using the initial condition (5.5) to get V^0, then use V^0 to update the jump condition (5.7) and get $\left[V^1\right]$, and again solve the Laplace problem with this new interface condition to obtain V^1, and so on. As mentioned in the previous section, for the Dirichlet condition (5.2) to be valid, the boundary $\partial\Omega$ should be chosen far enough from the cell, hence we choose a mesh with width 5 times larger than the diameter of the cell with refinement around the membrane. Another important choice is the time-step Δt, we used the same rules as in [14] which results in a choice of time-step of 0.3ns when the time constant of the electric pulse is about 5μs.

5.4. Numerical results. In the case of a spherical cell exposed to a rectangular electric pulse, it is possible to obtain the exact solution for the time evolution of the transmembrane voltage $[V]$ by means of the Laplace transform [9]. We computed numerically the potential V for a rectangular pulse of duration 5μs and compared our result with the exact solution in [9] (see Figure 5.2). The relative error in the maximum norm was 0.0154, and 0.0131 in the L^2-norm. This suggests that despite the fact that we used a straightforward discretization in time, the results are accurate provided we choose a small time-step.

In Figure 5.3, we represent the induced potential $(V - V_a)$ at different times during the polarization of the cell. We can clearly see that the maximum values of transmembrane potential (where electroporation would occur) are at the cathodic and anodic poles, this fact has also been observed experimentally. In fact it can be shown analytically that the transmembrane voltage has a distribution proportional to $\cos\theta$.

6. Conclusion. We presented a discontinuous Galerkin method for elliptic interface problems. Assuming that the interface lies on the mesh lines, we showed that the method is symmetric and optimally convergent in the L^2-norm, and confirmed the theoretical results by numerical experiments. In the case of static interface problems, there are several reasons why one may prefer a DG type approach over finite difference schemes. Firstly, just like boundary conditions, interface conditions play a significant role in the physical phenomenon. On the one hand, finite difference schemes usually have poor adaptivity and may fail to capture such phenomena completely. On the

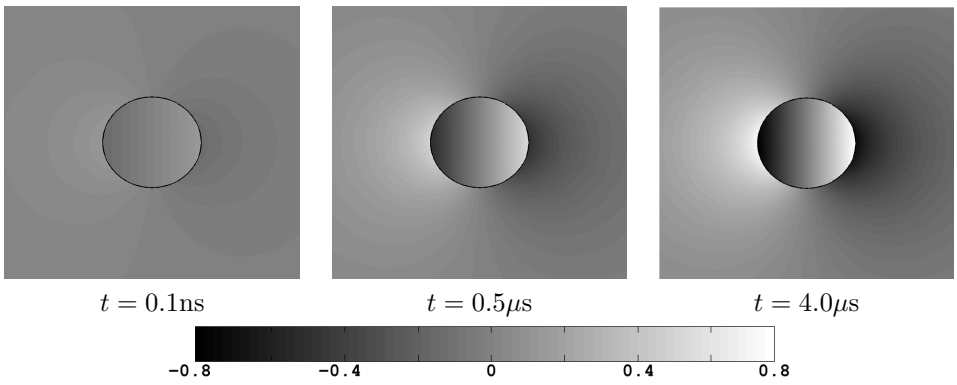

FIG. 5.3: Induced potential for a rectangular pulse

other hand, DG methods allow great flexibility in mesh adaptivity making it easy to refine the mesh whenever necessary. This suggests that DG methods may be valuable and may provide better solutions than standard schemes to that respect. Secondly, finite difference schemes are to our knowledge limited so far to second order accuracy while the method presented here provides higher order approximation as suggested by numerical experiments. Even though this method may be unpractical for moving interface problems, we have seen that interesting problems arise in computational biology in the form of elliptic interface problems with dynamic boundary conditions like the mathematical models of electroporation. The simulation made in this paper considered a model that did not include the biological phenomenon itself which occurs only when the threshold for the transmembrane potential is reached. However, recent mathematical models that take into account the formation of pores in the membrane take the same form as the one we studied. Furthermore, the discretization suggested in this paper can be easily extended to such models.

Acknowledgments. We would like to thank professor Schewchuk to make freely available to the research community his mesh generation software *Triangle* [16], with which we generated all triangulations used in our experiments.

REFERENCES

[1] D.N. Arnold, An interior penalty finite element method with discontinuous elements, SIAM J. Numer. Anal. 19 (1982), 742–760.
[2] D.N. Arnold, F. Brezzi, B. Cockburn and L.D. Marini, Unified analysis of discontinuous Galerkin methods for elliptic problems, SIAM J. Numer. Anal. 39 (2002), 1749–1779.
[3] J.H. Bramble and J.T. King, A finite element method for interface problems in domains with smooth boundaries and interfaces, Adv. Comput. Math. 6 (1996), 109–138.
[4] L.A. Cartee and R. Plonsey, The transient subthreshold response of spherical and cylindrical cell models to extracellular stimulation, IEEE T. Bio-med. Eng. 39 (1992), 66–85.
[5] P. Castillo, Performance of discontinuous Galerkin methods for elliptic PDEs, SIAM J. Sci. Comput. 24 (2002), 524–547.
[6] B. Cockburn and C.-W. Shu, The local discontinuous Galerkin method for time-dependent convection-diffusion system, SIAM J. Numer. Anal. 35 (1998), 2440–2463.
[7] R. Davalos, Y. Huang and B. Rubinsky, Electroporation: Bio-electrochemical mass transfer at the nano scale, Microscale Therm. Eng. 4 (2000), 147–159.
[8] S. Hou and X.-D. Liu, A numerical method for solving variable coefficient elliptic equation with interfaces, Preprint, 2002.

[9] T. Kotnik, D. Miklavčič and T. Slivnik, Time course of transmembrane voltage induced by time-varying electric fields–a method for theoretical analysis and its application, Bioelectroch. Bioener. 45 (1998), 3–16.
[10] R.J. Leveque and Z. Li, The immersed interface method for elliptic equations with discontinuous coefficients and singular sources, SIAM J. Numer. Anal. 31 (1994), 1019–1044.
[11] Z. Li, A fast iterative algorithm for elliptic interface problems, SIAM J. Numer. Anal. 35 (1998), 230–254.
[12] X.-D. Liu, R.P. Fedkiw, and M. Kang, A boundary condition capturing method for Poisson's equation on irregular domains, J. Comput. Phys. 160 (2000), 151–178.
[13] X.-D. Liu and T.C. Sideris, Convergence of the ghost fluid method for elliptic equations with interface, Math. Comp. 72 (2003), 1731–1746.
[14] A. Ramos, A. Raizer and J.L.B. Marques, A new computational approach to the electrical analysis of biological tissues, Bioelectrochemistry 59 (2003), 73–84.
[15] J.A. Roitberg and Z.G. Seftel, A homeomorphism theorem for elliptic systems, and its applications, Mat. Sb. 78 (1969), 446–472.
[16] J. Schewchuk, Triangle: a two dimensional quality mesh generator and Delaunay triangulator, Url:www.cs.cmu/˜quake/triangle.html.